Journal of Magnetic Resonance 298 (2019) 6–15

Contents lists available at ScienceDirect

Journal of Magnetic Resonance

journal homepage: www.elsevier.com/locate/jmr

Studies on NMR-signal up-conversion from radio-frequency to optical regimes using a lightweight nanomembrane transducer

Yusuke Tominaga [a], Kentaro Nagasaka [b], Koji Usami [b], Kazuyuki Takeda [a,*]

[a] Division of Chemistry, Graduate School of Science, Kyoto University, 606-8502 Kyoto, Japan
[b] Research Center for Advanced Science and Technology (RCAST), The University of Tokyo, Meguro-ku, Tokyo 153-8904, Japan

ARTICLE INFO

Article history:
Received 30 March 2018
Revised 10 November 2018
Accepted 12 November 2018
Available online 15 November 2018

Keywords:
Electro-Mechano-Optical (EMO) NMR
rf-to-light up-conversion
Membrane oscillator
Electro-mechanical coupling
Opto-mechanical coupling

ABSTRACT

Our recent report on Electro-Mechano-Optical (EMO) NMR proved the feasibility of up-conversion of NMR signals from radio-frequency to optical regimes using a metal-coated, high-Q membrane oscillator (Takeda et al., 2018). However, the signal-to-noise ratio, which can in principle exceed that of the conventional electrical detection scheme, was far below than ideal. Here, we developed an aluminum-coated membrane oscillator and used for a capacitor electrode as well as a mirror of an optical cavity. Compared to the gold-deposited membrane used in our previous study, the characteristic frequency of membrane oscillation was significantly higher due to mass reduction, leading to remarkable elimination of noise in the process of conversion of radio-frequency signals to the mechanical oscillation of the membrane. Taking advantage of the significantly improved EMO NMR, we explore physics behind it in terms of coherent transduction of electrical nuclear induction signals to mechanical and then to optical signals. In addition, we study the transient response of the membrane oscillator to electrical excitation due to nuclear induction.

1. Introduction

Recently, we put forth a new approach to detection of NMR through signal up-conversion from the radio-frequency (rf) to the optical regimes [1]. There, an elastic, high-Q, metal-coated membrane made of stoichiometric silicon nitride serves for both an electrode of a capacitor that is a part of an LC tank circuit, and a mirror of an optical cavity. The electromotive force due to nuclear induction exerts rf voltage between the electrodes of the membrane capacitor, causing the Coulomb force between them. Under application of the *drive* signal to the LC circuit, the electro-mechanical coupling develops between the LC circuit and the membrane oscillator. When the frequency of the drive signal is set at either the sum or the difference of the Larmor frequency and the membrane oscillation frequency, the nuclear induction signal can shake the membrane, and in turn, the membrane displacement changes the length of the optical cavity. Since the membrane oscillator and the optical cavity also interact with each other through the opto-mechanical coupling, the laser beam reflected back from the optical cavity can carry the nuclear induction signal.

In this electro-mechano-optical (EMO) NMR approach [1], the noise added through the process of signal up-conversion can in principle be made smaller than that in the conventional electrical detection approach [1,2]. However, in the first successful demonstration of EMO NMR, signal-to-noise ratio (SNR) was far below than that in the traditional approach, where the major limitation was ascribed to the noise imposed on the drive signal with the frequency rather close to the Larmor frequency, and it was suggested that the performance would be improved by increasing the frequency of characteristic oscillation of the membrane and thereby increasing the difference in the frequency between the drive signal and the Larmor frequency.

Here, we report significant improvement in the sensitivity of EMO NMR to the extent that our previous claim that EMO NMR *potentially* offers better transduction sensitivity compared to electrically detected NMR, which was far from ideal in our previous proof-of-principle report, has now been realistic. The idea is to reduce the weight of the metal-coated membrane, and thereby to increase the characteristic frequency ω_m of membrane oscillation. In the following, we describe our new experimental setup for EMO NMR, and demonstrate sensitivity-improved EMO NMR experiments. As we will discuss below, the increase in SNR is due to the reduced phase noise of the drive signal. Based on the sensitivity-improved EMO NMR data, we explore physics behind NMR signal transduction from rf to optical regimes, such as coherent signal transfer and transient response of the membrane oscillator.

* Corresponding author.
E-mail address: takezo@kuchem.kyoto-u.ac.jp (K. Takeda).

https://doi.org/10.1016/j.jmr.2018.11.003
1090-7807/

2. Principle

In EMO NMR, the nuclear induction signal is transduced in the following two steps. First, the electro-mechanical coupling between the LC circuit and the membrane oscillator converts the voltage signal to the mechanical motion of the membrane. Then, the opto-mechanical coupling between the membrane oscillator and the optical cavity modulates the light according to the mechanical motion of the membrane. The important parameters that characterize the efficiency of signal transfer include the electro-mechanical cooperativity $\mathcal{C}_{\rm em}$, the rate of dissipation $\gamma_{\rm i}$ in the LC circuit, the LC input coupling constant $\kappa_{\rm i}$, opto-mechanical cooperativity $\mathcal{C}_{\rm om}$, the optical dissipation rate $\gamma_{\rm o}$, and the optical output coupling constant $\kappa_{\rm o}$, giving the signal transfer rate proportional to [1]

$$\mathcal{C}_{\rm om}\frac{\kappa_{\rm o}}{\kappa_{\rm o}+\gamma_{\rm o}}\mathcal{C}_{\rm em}\frac{\kappa_{\rm i}}{\kappa_{\rm i}+\gamma_{\rm i}}, \tag{1}$$

where, for an impedance-matched circuit, the critical-coupling condition $\frac{\kappa_{\rm i}}{\kappa_{\rm i}+\gamma_{\rm i}}=\frac{1}{2}$ holds. Using the opto-mechanical coupling strength $G_{\rm om}$ and the electro-mechanical coupling strength $G_{\rm em}$, the cooperativities are represented as

$$\mathcal{C}_{\rm om}=\frac{G_{\rm om}^2}{\gamma_{\rm m}(\kappa_{\rm o}+\gamma_{\rm o})}, \tag{2}$$

$$\mathcal{C}_{\rm em}(\omega)=\frac{4G_{\rm em}^2}{\gamma_{\rm m}}\frac{\kappa_{\rm i}+\gamma_{\rm i}}{4\omega^2+(\kappa_{\rm i}+\gamma_{\rm i})^2}. \tag{3}$$

The electro-mechanical coupling strength $G_{\rm em}$ increases with the amplitude V_0 of the drive signal, so that the electro-mechanical cooperativity $\mathcal{C}_{\rm em}$ is proportional to the drive power $P_{\rm D}$; theoretical formula for $G_{\rm em}$ is given by [1]

$$G_{\rm em}=\frac{V_0}{2}\frac{\omega_{\rm LC}^2}{\omega_{\rm LC}^2-\omega_{\rm D}^2}C(z_0)\left(\frac{\partial}{\partial z}\frac{1}{C(z_0)}\right), \tag{4}$$

where $\omega_{\rm D}$ is the frequency of the drive signal, $\omega_{\rm LC}$ is the resonance frequency of the LC circuit, $C(z)$ is the displacement (z)-dependent capacitance of the membrane module, and z_0 is the equilibrium distance between the electrodes of the capacitor. In practice, singularity in Eq. (4) for $\omega_{\rm D}=\omega_{\rm LC}$ is avoided due to the presence of dissipation in the system.

In both the EMO and the conventional schemes, the Johnson noise developing in the tank circuit is faithfully transduced. Conversely, difference in the sensitivity arises from other sources of noise. That is, in EMO NMR, thermal fluctuation of the membrane oscillator is also converted to light, whereas in the conventional approach, the additional noise comes from the preamplifier. Importantly, noise due to membrane thermal fluctuation is converted to light only in *a single* step through the opto-mechanical coupling. Now the transduction of the membrane displacement noise is characterized through

$$\mathcal{C}_{\rm om}\frac{\kappa_{\rm o}}{\kappa_{\rm o}+\gamma_{\rm o}}. \tag{5}$$

It follows from Eqs. (1) and (5) that, as the electro-mechanical cooperativity $\mathcal{C}_{\rm em}$ increases, the relative contribution of the transduced nuclear induction signal becomes significant compared to the thermal fluctuation of the membrane. Eventually, the contribution of the former can overwhelm that of the latter, and ultimately, the SNR can be better than that in the conventional electrical detection of NMR, where the noise added through the process of electronic signal amplification is characterized by the noise temperature of the preamplifier. Since $\mathcal{C}_{\rm em}$ increases with the power of the drive signal, it is desirable to apply intense drive signal to the extent that its phase noise at the Larmor frequency lies below the noise floor of the system. It is also worth pointing out that reducing the gap d between the electrodes of the membrane capacitor is very effective, as the electro-mechanical coupling strength $G_{\rm em}$ is proportional to d^{-2} [1], and hence the electro-mechanical cooperativity $\mathcal{C}_{\rm em}$ scales as d^{-4}.

Another formula for the eletro-mechanical coupling strength [1],

$$G_{\rm em}=\frac{1}{2}g_{\rm em}\sqrt{\frac{P_{\rm D}}{\hbar\omega_{\rm LC}(\kappa_{\rm i}+\gamma_{\rm i})}}, \tag{6}$$

is instructive; $\frac{1}{2}$ in Eq. (6) stems from the rotating-wave approximation, $g_{\rm em}$ is the single-photon electro-mechanical coupling rate, and $\sqrt{P_{\rm D}/(\hbar\omega_{\rm LC}(\kappa_{\rm i}+\gamma_{\rm i}))}$ is the square root of the photon number of the drive signal in the LC circuit. The opto-mechanical coupling strength can be represented in a similar way. That is, using the single-photon opto-mechanical coupling rate $g_{\rm om}$ and the intracavity photon number $\mathcal{N}$ of the optical drive,

$$G_{\rm om}=\frac{1}{2}g_{\rm om}\sqrt{\mathcal{N}}. \tag{7}$$

The single-photon opto-mechanical coupling rate is represented using the zero-point fluctuation $z_{\rm zpf}=\sqrt{\hbar/(2m\omega_{\rm m})}$, with m being the effective mass of the membrane and $\omega_{\rm m}$ being the frequency of characteristic oscillation, as

$$g_{\rm om}=\Omega_{\rm c}\frac{z_{\rm zpf}}{l}, \tag{8}$$

where $\Omega_{\rm c}=2\pi c/\lambda$ and l are the resonance frequency and the length of the optical cavity. Similarly, the single-photon electro-mechanical coupling rate is given by

$$g_{\rm em}=\omega_{\rm m}\frac{z_{\rm zpf}}{2d}\eta. \tag{9}$$

Here, η is the participation ratio, which measures the contribution of the capacitance of the membrane module with respect to the total capacitance of the tank circuit. Since η is proportional to the capacitance of the membrane module and is thereby inversely proportional to the capacitor gap $d, g_{\rm em}\propto d^{-2}$. It follows that the electro-mechanical coupling strength $G_{\rm em}$ is also proportional to d^{-2}.

In the case of critical coupling for the LC circuit, and for a given set of spectral densities S (nuclear induction), S_{qq} (Johnson noise), S_{FF} (membrane thermal fluctuation), $\{S_{XX}, S_{YY}\}$ (quadratures of optical shot-noise), the overall SNR within a bandwidth Δ around the frequency $\omega_{\rm m}$ of characteristic oscillation of the membrane is represented as

$$\frac{S}{\sqrt{2\Delta}}\left[\frac{S_{XX}(\omega_{\rm m})+S_{YY}(\omega_{\rm m})}{2\mathcal{C}_{\rm om}\frac{\kappa_{\rm o}}{\kappa_{\rm o}+\gamma_{\rm o}}\mathcal{C}_{\rm em}(\omega_{\rm m})}+\frac{2S_{FF}(\omega_{\rm m})}{\mathcal{C}_{\rm em}(\omega_{\rm m})}+S_{qq}(\omega_{\rm m})\right]^{-\frac{1}{2}}. \tag{10}$$

3. Experiment

3.1. Mirror/capacitor fabrication

Metal-coated silicon nitride (Si_3N_4) membranes were fabricated in the same way as described in Ref. [1], except that the material deposited on the membrane has been changed from gold to aluminum. Fig. 1 schematically describes the geometry of the membrane and the membrane capacitor. On a Si_3N_4 membrane with a lateral size of 500 × 500 μm and a thickness of 50 nm (Fig. 1(a)), a circular layer of aluminum with a diameter of 450 μm and a thickness of 100 nm was vacuum deposited (Fig. 1(b)). For the counter electrode of the capacitor, a pattern, as depicted in Fig. 1

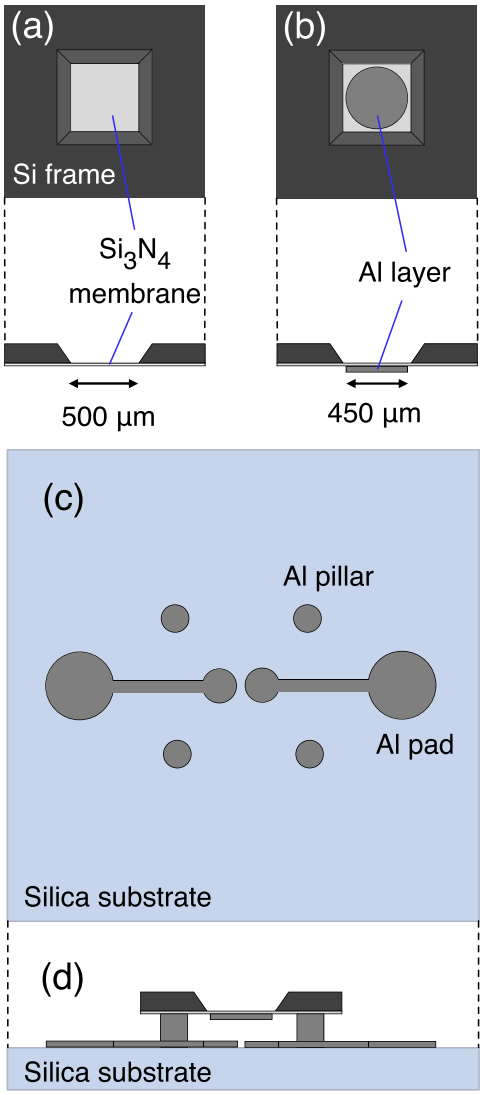

Fig. 1. (a) A window of stoichiometric Si_3N_4 membrane (500 × 500 μm) stretched over a silicon frame (QX5050AS, Norcada). On the membrane a circular aluminum layer was deposited, as described in (b). In addition, a silica glass was employed, and patterns, as depicted in (c), were vacuum deposited with aluminum. (d) A schematic side view of the membrane capacitor fabricated by piling the membrane frame onto the silica substrate.

(c), was deposited with aluminum on a silica substrate. In addition, four aluminum pillars with a height of 800 nm were made by vacuum deposition to support the frame of the membrane. In clean environment, the membrane was gently piled on the substrate (Fig. 1(d)) to assemble the capacitor.

The value of the capacitance can be estimated from a crude but simple model of a parallel-plate capacitor. The capacitance, C, is given by

$$C = \frac{A\epsilon_0}{d}, \tag{11}$$

where A is the area of the plate, ϵ_0 is the permittivity of free space, and d is the capacitor gap. Here, an equivalent circuit is a pair of capacitors connected in series, and with the diameter ($\sim$ 160 μm) of the counter electrodes on the glass substrate, C is roughly estimated to be ca. 0.1 pF for $d = 800$ nm.

To avoid damping of mechanical oscillation due to air friction, the membrane capacitor was put in a home-made 200 × 200 × 200 mm vacuum chamber equipped with a pair of hermetically sealed rf ports and a transparent window for electrical and optical accesses from outside, respectively.

3.2. Setup

The detailed configuration of the experimental setup, as schematically described in Fig. 2, was extensively described in Ref. [1]. All experiments were performed at room temperature. For NMR experiments, a home-built rf circuits, and an Opencore NMR spectrometer [3–5] were used.

3.2.1. Optical setup

As the source of light, a 1064 nm laser (Mephisto S, Coherent) was employed. We built a hemispherical optical cavity composed of the aluminum *mirror* on the Si_3N_4 membrane (Fig. 2(a)) and a concave mirror (Fig. 2(b)) with a radius of curvature of 50 mm and reflectance of 95%. The latter was attached to a ring piezo actuator (Fig. 2(c)) for fine adjustment of the cavity length. Based on Gaussian optics, we designed a cavity such that the cavity length and the beam diameter of the membrane were 47.3 mm and 0.124 mm, respectively. The laser beam was applied continuously into the optical cavity throughout the experiments, and the light reflected back from the cavity was differentially detected with respect to the incident light using a pair of photo detectors (PDA20C, Thorlabs) (Fig. 2(d) and (e)). Fig. 3 shows the noise-floor level of the differentially detected optical signal as a function of the intensity of the incident laser beam. Here, the slope would be unity under shot-noise limited photo-detection, while it would be 2 for classical-laser-noise limited detection [6]. The slope 1.1 in the present result indicates that our differential optical detection was close to ideal.

3.2.2. Electrical setup

We wound a pair of separate coils with insulator-coated copper wires for signal reception and pulse application. The receiving coil (Fig. 2(f)) was an 8-turn solenoid coil with a diameter of 3 mm. The ends of the coils were electrically connected to the electrodes of the membrane capacitor placed inside the vacuum chamber through a pair of hermetically sealed ports. A trimmer-capacitor (Fig. 2(g)) was added in parallel to make an LC circuit resonate at 42.74 MHz. Using additional trimmer capacitors (Fig. 2(h) and (i)), the circuit was differentially impedance matched to 50 Ohm, and converted to the single-ended mode using a 180 degree splitter (Fig. 2(j)).

The transmitting coil (not shown in Fig. 2 for clarity) was a 2 turn saddle coil placed just outside the receiving coil, and impedance-matched at the same frequency using separate trimmer capacitors (not shown in Fig. 2). The Q factors of the receiving and transmitting tank circuits were measured to be 25 and 14, respectively, and the isolation between the transmitting and the receiving LC circuits was 22.6 dB. We did not observe any arcing events for excitation-pulse powers of up to 8.5 W. We did not do destruction experiments with even higher powers, since fabrication of the membrane module is technically demanding, and reproduction is a rather formidable task.

3.2.3. NMR setup

In this work, we employed a nominally 1 T permanent magnet, aiming at observing ^{1}H NMR signals at frequencies around 42.6 MHz. 0.1 M aqueous solution of $CuSO_4$ was put in a glass test tube with an inner diameter of 1 mm, and was used as a sample.

For EMO NMR, a low-noise amplifier (N141-305AA, THAMWAY) (Fig. 2(k)) was used to send the drive signal through the port of the receiving LC circuit. That is, the drive signal generated by a direct-digital synthesizer (Fig. 2(l)) was amplified by this low noise

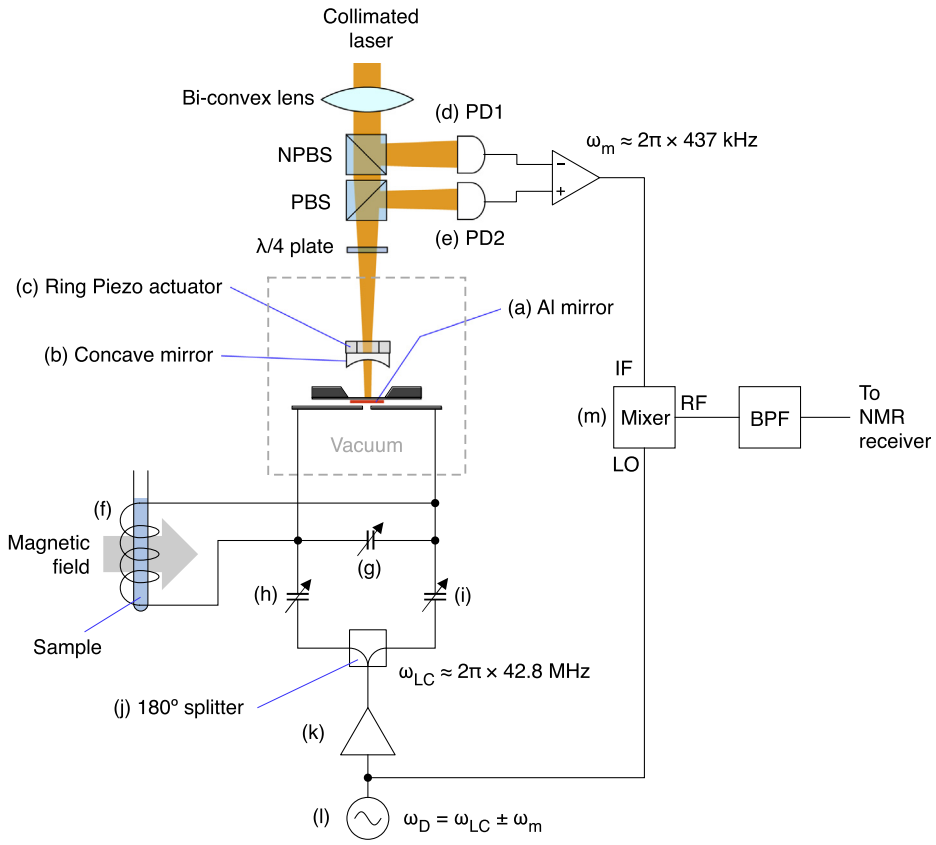

Fig. 2. A diagram of experimental setup for EMO NMR. The glossary is as follows. NPBS: Non-polarizing beam splitter, PBS: Polarizing beam splitter, PD: Photo detector, BPF: Band-pass filter.

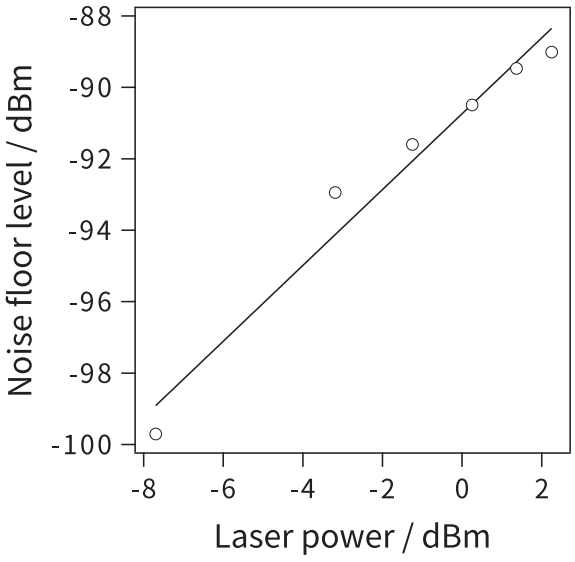

Fig. 3. Laser-power dependence of the noise floor in differentially detected optical signals. The solid line represents linear fitting (slope: 1.1).

amplifier, and its *output* port was connected to the receiving tank circuit. Conversely, when we performed the conventional, electrical NMR signal detection for comparison, the direction of the low-noise amplifier was reversed, so that the nuclear induction signal was amplified before being sent to the receiver of the NMR spectrometer. In this work, we used our best available low-noise amplifier operating at room temperature. Its noise figure was measured to be 1.1 dB (noise temperature: 84 K).

Under application of the drive signal, the rf signal developed in the receiving LC circuit is expected to surf on the optical carrier through two coupling steps: first, the electro-mechanical coupling between the LC circuit and the membrane oscillator, and second, the opto-mechanical coupling between the optical cavity and the membrane oscillator. Here, the rf signal was either a *tone* signal, i.e., a synthesized continuous-wave signal intentionally applied to the circuit for diagnosis purposes, or the electromotive force due to nuclear induction.

For the tone experiments, the photo-detected signal was directly sent to a spectrum analyzer to obtain the power spectrum of the light-converted rf signal through the membrane oscillation.

Conversely, for EMO NMR where coherent signal acquisition is of interest, a mixer (ZFM-3+, Mini-Circuits) (Fig. 2(m)) was employed, and the signal from the photo-detectors was sent to the IF port of the mixer, whereas the branched drive signal was sent to its LO port. As a result, the signal coming out of the RF output port is expected to carry the NMR signal at the original Larmor frequency, so that the signals can be acquired and accumulated using an NMR spectrometer.

4. Results and discussions

4.1. Membrane spectrum

The power spectrum shown in Fig. 4(a) was obtained from the signal coming out of the photo-detectors that received the laser beam reflected back from the optical cavity with no electro-mechanical coupling. We found a peak at 434.7 kHz, and assigned it to be the fundamental drum mode of membrane oscillation with an opto-mechanical coupling. In our previous work where we

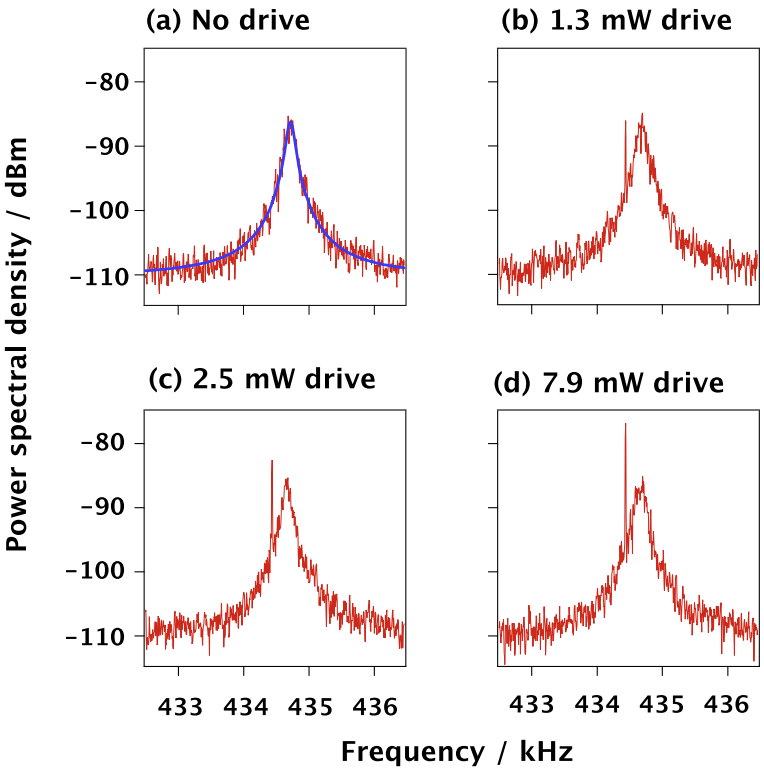

Fig. 4. Optically detected membrane spectra showing the fundamental drum mode of mechanical oscillation at 434.7 kHz. The data in (a) was obtained without the drive signal applied to the LC circuit, while those in (b)–(d) were acquired with the drive signal with powers of 1.3, 2.5, or 7.9 dBm in the presence of a tone signal such that it results in the power of −86 dBm in the receiving LC circuit. The data were obtained by detecting the laser beam reflected back from the optical cavity and using a spectrum analyzer with a resolution bandwidth of 10 Hz and a video bandwidth of 1 Hz. The incident laser power was 0.38 mW. The blue line in (a) shows a Lorentzian curve with a width of 130 Hz. For comparison, the tone signal was measured electrically by connecting the rf port of the receiving circuit to a spectrum analyzer (resolution bandwidth 10 Hz, video bandwidth 1 Hz) (e) with no amplifier, and (f) with a low-noise amplifier (gain 30 dB, noise figure 1.1 dB).

employed the much heavier Au-coated membrane oscillator with the same dimension, the fundamental mode was found at 180 kHz. Thus, the characteristic frequency of mechanical oscillation was higher by a factor of ca. 2.4 in the present work. From Lorentzian curve fitting (blue line in Fig. 4(a)), the width of the oscillation mode was obtained to be 130 Hz.

For a square membrane with a side length l and a density ρ_{SiN}, the characteristic frequency $\nu_{\mathrm{m}}(j,k)$ of the (j,k) drum mode is given by

$$\nu_{\mathrm{m}}(j,k) = \sqrt{\frac{T}{4\rho_{\mathrm{SiN}}l^2}}\sqrt{j^2+k^2}, \tag{12}$$

where T is the tensile strength of the membrane [7]. Here, we assume the boundary conditions where the four sides of the membrane are fixed. For the fundamental $(1,1)$ mode, the oscillation frequency $\nu_{\mathrm{m}} = \nu_{\mathrm{m}}(1,1)$ is represented as

$$\nu_{\mathrm{m}}(1,1) = \sqrt{\frac{T}{2\rho_{\mathrm{SiN}}l^2}}. \tag{13}$$

For the Si_3N_4 membrane that we used in this work, the nominal tensile strength T is 0.9 GPa. From the density $\rho_{\mathrm{SiN}} \approx 2.7\times10^3$ kg/m^3 of silicon nitride, the frequency of the mechanical oscillation of the bare membrane, i.e., the membrane without metal coating, is estimated to be 816 kHz.

Since the metal layer adds the mass to the Si_3N_4 membrane determined by the density ρ_{metal} of the metal (Au or Al) and its volume V, the effective density ρ' of the metal-coated membrane is calculated by

$$\rho' = \rho_{\mathrm{SiN}}\left(1+\frac{\rho_{\mathrm{metal}}}{\rho_{\mathrm{SiN}}}\frac{V}{l^2h}\right), \tag{14}$$

where $h = 50$ nm is the membrane thickness. Here, we have assumed that the metal layer uniformly distributes over the membrane surface approximately. For the gold layer, the effective density ρ' is ca. $10.1\rho_{\mathrm{SiN}}$, which would decrease the characteristic frequency of the membrane oscillation by a factor of $\sqrt{10.1} \approx 3.18$, i.e., to $820/3.18 \approx 260$ kHz for the fundamental mode, whereas for the Al layer of the same dimension, the effective density can be as low as $2.27\rho_{\mathrm{SiN}}$, and the estimated fundamental frequency would be 540 kHz. Considering the crudeness of the assumption we made and the uncertainty of the actual layer thickness, this can explain the measured frequency of ca. 180 kHz and 430 kHz of the Au-coated and the Al-coated membrane, respectively.

One drawback of the Al layer would be the lower light reflectivity (95% at 1064 nm) compared to that of the Au layer (99%). Nevertheless, as shown below, the higher frequency of mechanical oscillation of the lightweight membrane can much more than compensate for the degradation of the optical performance.

In this work, the pressure inside the vacuum chamber was reduced to 8×10^{-4} Torr using a turbo molecular pump. Under higher pressure, the membrane spectrum showed much broader peak, and the peak was not discernible at atmospheric pressure.

4.2. Tone measurements

To verify the performance of the membrane transducer, we examined light-conversion of a tone rf signal applied through the port of the transmitting tank circuit. Here, by taking the isolation (22.6 dBm) between the two circuits into account, we applied a tone signal such that it resulted in the power of the tone signal in the receiving LC circuit to be −86 dBm, which corresponds to

the rf power generated by the electromotive force due to proton induction in our NMR experiment (see below). In the optical rf detection, we applied the drive signal at frequency $\omega_D = 2\pi \cdot 43.175$ MHz corresponding to $\omega_m + \omega_{LC}$ through the rf port of the receiving circuit. As demonstrated in Fig. 4(b)–(d), we found the tone peak superimposed on the membrane spectrum. This indicates that the tone rf signal was successfully up-converted into light.

The intensity of the tone peak increased with the power of the drive signal applied to the LC circuit. Importantly, we found no appreciable change in the noise floor level. This result contrasts our previous work [1] using the Au coated membrane, where the frequency ω_D of the drive signal was so close to the NMR frequency due to the low membrane frequency that the increased drive-signal intensity enhanced not only the signal, but also, unfortunately, noise.

The drive-power dependence of the tone spectrum allows us to extract both the opto-mechanical operativity $\mathcal{C}_{om}$ and the electro-mechanical cooperativity $\mathcal{C}_{em}$. Using the same procedure as described in Ref. [1], we obtained $\mathcal{C}_{om} = 2.4 \times 10^{-4}$ and $\mathcal{C}_{em} = 9.6 \times 10^{-4}$, which are comparable to those in the previous work.

4.3. NMR measurements

Using the experimental setup described above, we performed EMO signal detection of ^{1}H spin echoes in water in a 1 mm test tube. In advance, we examined the conventional, electrical ^{1}H NMR experiments by applying rf pulses through the transmit circuit and then by electrically detecting nuclear induction signals coming out of the port of the receiving circuit, and found out that the electromotive force caused the power of the induction signal to be −86 dBm at the spin-echo top.

Then, we switched to the EMO NMR detection, by applying the drive signal through the rf port of the receiving circuit, and detecting the optical signal reflected from the membrane optical cavity. Fig. 5(a) shows the spin-echo signal obtained by the EMO scheme. Here, the drive signal was continuously applied throughout the experiment, but during the rf pulses the frequency of the drive signal was detuned by 400 kHz to prevent the rf pulses from being converted to light. We did not switch on/off the drive signal, to avoid abrupt change in the photon number of the drive signal in the resonant circuit.

Compared to our previous, the first proof-of-principle demonstration of EMO NMR (Fig. 5(b)), the SNR was improved by a factor of 20.7 per scan. As shown below, this is ascribed to the increased frequency of the characteristic oscillation of the membrane by the factor of 2.4, preventing the NMR signal from being overwhelmed by the phase noise of the drive signal, whose frequency has now got further away from the Larmor frequency.

In semiconductor devices, random fluctuations of the charge density causes flicker (1/f) noise [8]. In the present case, the 1/f noise appears as sidebands around the drive signal at $\omega_D/2\pi$. As a result of amplification in the feedback loop of the oscillator, the power spectral density of the oscillator's output has the phase noise components proportional to $1/f^3$ (−9 dB/octave) for offset frequencies relatively close to the carrier frequency, and those proportional to $1/f$ (−3 dB/octave) for relatively higher offset frequencies [9]. The corner frequency at which the effect of phase noise becomes negligible can be as high as several MHz for GaAs devices [8].

Fig. 6 shows the profile of the measured phase noise of the drive signal of a direct-digital synthesizer (DDS) using AD9858 (Analog Devices) that was actually used for the EMO experiments. We found that the offset frequency (ca. 180 kHz) corresponding to

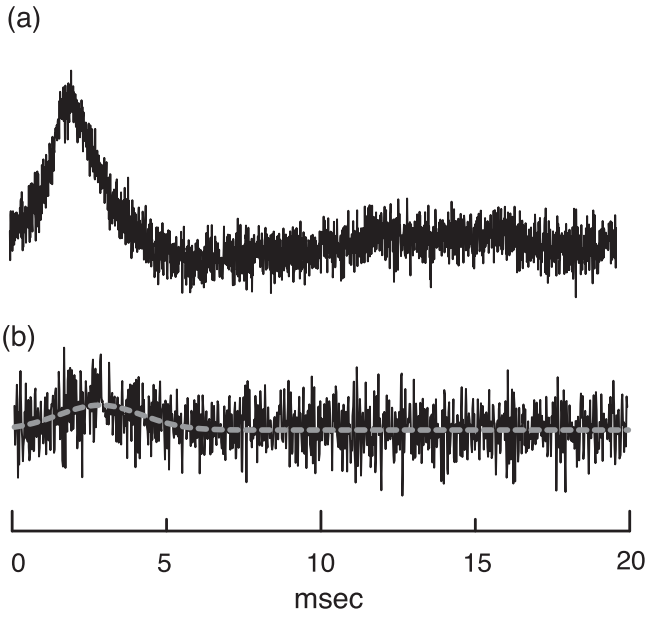

Fig. 5. (a) A ^{1}H spin echo signal in 0.1 M aqueous solution of $CuSO_4$ acquired by the EMO scheme with the aluminum-coated silicon nitride membrane. The magnetic field was 1 T. The interval between the $\pi/2$ and π pulses was 1.5 ms. Drive power was 10 dBm, and the signal was accumulated over 1000 times. (b) An EMO-detected ^{1}H spin echo from the same sample but acquired over 5000 times with the gold-coated silicon nitride membrane [1]. The broken line represents a fitted curve with a Gaussian function.

the characteristic frequency of mechanical oscillation in the previous work is in the region of $1/f^3$ dependence, whereas that (ca. 430 kHz) to the mechanical frequency in the present work barely reached the point where the phase noise begins to scale with $1/f$. Indeed, the level of the phase noise in the present work was found to be lower than that in the previous work by a factor of 13.4 dB. Then, the improvement in SNR due to the reduced phase noise is estimated to be $10^{13.4/10} \approx 21.9$, which is consistent with the actual increase in SNR (20.7).

For reference, we examined a power spectrum of the tone signal with a power of −86 dBm obtained with a spectrum analyzer connected to the rf port of the receiving circuit (Fig. 7(a)). Fig. 7(b) shows data obtained with the EMO scheme, in which the on-resonance tone signal was acquired. Here, the EMO data, which indicated that the sensitivity was lower compared to that in the electrical detection by four orders of magnitude, was acquired in a different experimental run with the degraded membrane oscillator presumably due to aging or dust contamination; the width of the thermal vibration of the oscillator was 2900 Hz (Fig. 7(c)), which was larger by a factor of ca. 22 than that when any other data shown in this paper were acquired. Since the rate γ_m of damping of the membrane oscillator corresponds to 2π times this width, and since both the opto-mechanical cooperativity $\mathcal{C}_{om}$ and the electro-mechanical cooperativity $\mathcal{C}_{em}$ scales inversely with γ_m (see Eqs. (2) and (3)), the level of the EMO signals in other data ought to have higher by $22^2 \sim 500$. Still, the overall sensitivity of the measurement of the continuous-wave signal detected by the EMO approach is expected to be orders of magnitude lower than that in the electrical detection. To offer better sensitivity, the electro-mechanical cooperativity $\mathcal{C}_{em}$ needs to be enhanced in future works by reducing the gap d between the electrodes of the membrane capacitor, which would scale the electro-mechanical cooperativity $\mathcal{C}_{em}$ as d^{-4}. Interestingly, in contrast to the continuous-wave signals, transient signals detected by the

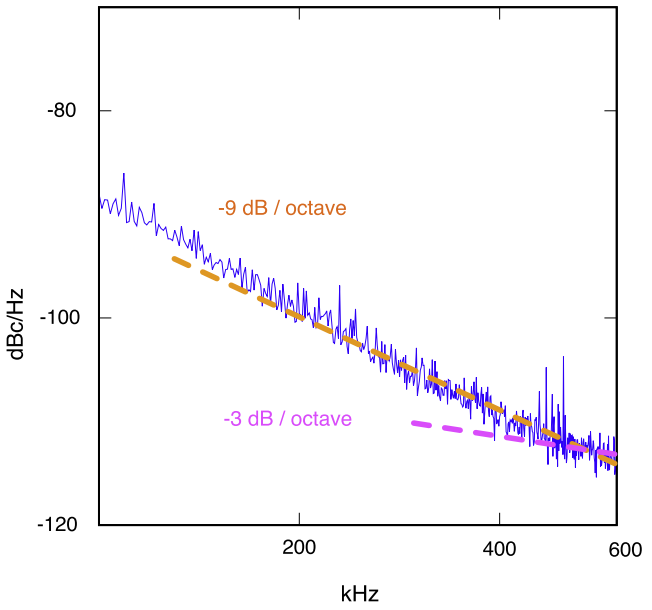

Fig. 6. Phase noise of the drive signal generated by a DDS synthesizer using AD9858 (Analog Devices) as a function of the offset frequency. The data was obtained by mixing a 10 dBm drive signal at 43.17 MHz with a reference signal at the same frequency, and then passing the IF signal through a 10 MHz low-pass filter, and finally monitoring the resultant signal with a spectrum analyzer with a resolution bandwidth of 10 Hz. Lines with slopes of −9 dB/octave and −3 dB/octave are also shown to guide the eye.

EMO scheme showed comparable sensitivity to that in the electrical detection, as demonstrated below.

Nevertheless, the sensitivity has now significantly been improved, and we can explore the fundamental aspects of EMO NMR. In the following, we study the coherent nature of transduction of the electrical NMR signal into the mechanical and then into the optical signal, and the transient response of the membrane oscillator to the electrical input.

4.4. Coherent nature of the EMO NMR signals

In our work on EMO signal transduction, we relied on the amplitude modulation of the optical signal. We thus required that the membrane displacement changes the intensity of light reflected back out of the optical cavity. Accordingly, we adjusted the distance between the mirrors of the optical cavity such that the optical cavity was deliberately detuned approximately by half width of the resonance line. Since one of the mirrors was attached on a ring piezo actuator, fine tuning of the cavity distance was done through adjustment of the voltage applied to the piezo device.

Fig. 8(a) shows the cavity-length dependence of the laser reflectance. We now have a pair of options to detune the optical cavity. One is to increase the distance between the mirrors compared to the resonance condition corresponding to the position of the dip in Fig. 8(a). For a cavity length indicated by the broken red line in Fig. 8(a), the slope of the tangential line is positive, and the effect of additional tiny positive displacement of the membrane is to increase the cavity reflectance. Conversely, in the condition where the cavity length is set shorter than that at the exact resonance, the slope of the tangential line has the opposite sign. Hence, the phase of the transduced NMR signals for these two configurations ought to be inverted with respect to each other.

Fig. 8(b) shows a spin-echo signal obtained by the EMO scheme with a cavity length indicated by the red broken line in Fig. 8(a), i.e., the longer cavity length than that of the exact resonance. When we changed the cavity length alone to that corresponding to the blue broken line in Fig. 8(a) while keeping all other experimental parameters unaltered, we observed the phase-inverted EMO NMR signal, as demonstrated in Fig. 8(c). These data indeed confirm the coherent nature of the NMR signal transferred to the motional perturbation to the membrane oscillator.

For the power of the incident laser beam exceeding 1 mW, we observed damping/enhancing of the peak of membrane thermal vibration spectrum depending on the cavity-detuning condition. Such interesting laser-cooling/heating effects, well known in the field of opto-mechanics [10], are to be explored in our future work in the context of EMO NMR.

4.5. Comparison between the EMO and the conventional NMR signals

For comparison, we also performed the conventional electrical NMR detection using the identical sample, and excitation/detection tank circuits under common experimental parameters. Figs. 9 (a) and (b) show electrically detected free induction decay excited by a single-pulse sequence and its Fourier-transformed spectrum. Here, the major origin of the signal decay with a time constant T_2^* of 0.44 ms, and thereby of the width $1/(\pi T_2^*)$ of 730 Hz of the resonance line is field-inhomogeneity of the permanent magnet that we used.

Fig. 9(c) was taken with the EMO detection scheme with drive power of 10 dBm, and Fig. 9(d) shows its Fourier-transformed spectrum. Here, the vertical scales of the spectra in Fig. 9 were adjusted such that the noise levels match. We observed different profile of the EMO NMR signal, as compared to that of the NMR signal detected through the conventional, electrical means. Such distortions can be explained by the transient response of the system, especially that of the membrane.

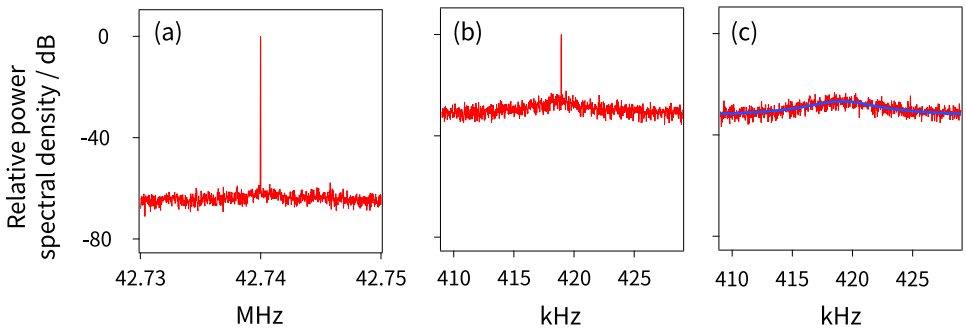

Fig. 7. (a) Relative power spectral density of an electrically detected tone signal at 42.74 MHz with a level of −86 dBm. (b) Relative power spectral density of the transduced tone signal detected by the EMO scheme with a drive power of 10 dBm. Data are normalized with respect to the level of the tone signal. (c) Power spectral density of membrane oscillation acquired without the tone signal. Lorentzian fitting with a width of 2930 Hz is also shown.

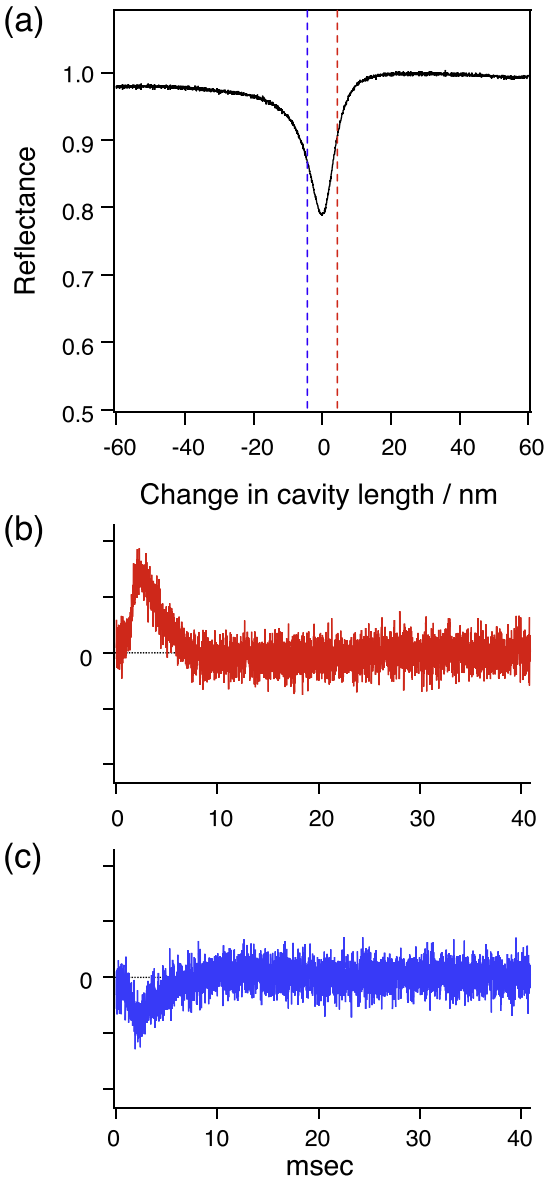

Fig. 8. (a) Laser-beam reflectance as a function of the cavity length. The vertical broken red and blue lines indicate the position detuned from the resonance to acquire ^{1}H EMO NMR signals in water shown in (b) and (c), respectively. Note that all other experimental conditions, except for the optical-cavity detuning positions, were identical. (For interpretation of the references to color in this figure legend, the reader is referred to the web version of this article.)

For a linear system, which we believe is the case for the current membrane oscillator, the response $b(t)$ to an excitation $a(t)$ is given by a convolution

$$b(t) = h(t) * a(t) \equiv \int_{-\infty}^{\infty} d\tau h(t-\tau)a(t), \tag{15}$$

where $h(t)$ is the response function of the membrane that characterizes its behaviour upon any excitations. Since the thermal spectrum of the membrane, like that seen in Fig. 4(a), showed the Lorentzian profile, now with a width of 100 Hz, we approximate $h(t)$ to be an exponential function with a time constant of $T_m = 2/(2\pi \times 100\ \text{Hz}) = 3.2$ ms. Thus, upon knowledge of the profile $a(t)$ of the original nuclear induction signal, the output of the membrane signal, and thereby EMO-detected signal, can be calculated straightforwardly from Eq. (15), or conversely, the NMR signal can be obtained from the measured EMO NMR signal by performing deconvolution.

In the present case, the profile of our ^{1}H signal in the time domain is approximated by an exponential function with the time constant T_2^* of 0.44 ms. Then, we can calculate analytical formula for convolution with a pair of exponential functions to be

$$b(t) = \frac{T_m T_2^*}{T_m - T_2^*}\left(e^{-t/T_m} - e^{-t/T_2^*}\right), \tag{16}$$

for $T_m > T_2^*$, and

$$b(t) = te^{-t/T_m} \tag{17}$$

for $T_m = T_2^*$. Eq. (16) explains well the measured EMO signal in the time domain that increased at the beginning, reached the maximum, and finally decayed. From Eq. (16), the time t_{max} that gives the maximum is calculated to be

$$t_{max} = \frac{T_m T_2^*}{T_m - T_2^*} \ln\left(\frac{T_m}{T_2^*}\right). \tag{18}$$

Using the parameters $T_m = 3.2$ ms and $T_2^* = 0.44$ ms, t_{max} is predicted to be 1.0 ms, which is satisfactorily consistent with the data obtained in Fig. 9.

In the frequency domain, the effect of this transient response is to reduce the bandwidth of the spectral range that can be covered, as seen in Fig. 9(d). Nevertheless, when the data were scaled to give the common noise intensity, the signal detected with the EMO scheme was comparable to that of the conventional electrical detection. The reason for obtaining the comparable sensitivity in the transient experiments, although the EMO detection of the continuos-wave tone signal resulted in orders-of-magnitude lower sensitivity as seen above, is to be studied in future works. A possible explanation is that the switching of the drive frequency during the rf pulses might have caused transient reduction in the gap between the electrodes of the membrane capacitor, and the electro-mechanical cooperativity had been increased temporarily.

From the practical point of view, some may argue that the limited bandwidth and spectral distortion can be problems, in particular in the context of broadband NMR analysis in chemical/biological applications. Nevertheless, we expect that the EMO NMR approach will find interest in field-sweep NMR experiments, where the frequency of the excitation/detection circuits is fixed so that and the external magnetic field is widely swept instead of scanning the resonance lines over a wide spectral range. Even though such an approach was indeed popular in the old days of NMR, and currently used in solid-state physics, recent emergence of high-field and high-resolution field-swept NMR would be of relevant [11,12]. In addition, one may encounter signal distortion due to the limited bandwidth even in the conventional NMR approach in future, considering recent remarkable progress in the development of high-Q probes using a cryogenically cooled or superconducting rf coils.

5. Summary and prospects

In the setup of EMO NMR, the material for the metal layer deposited on the membrane has been changed from gold to aluminum. As a consequence of this revision in the design and fabrication of the metal-coated membrane, its weight was significantly reduced, and the characteristic frequency of mechanical oscillation increased. The effect of the higher membrance frequency is to increase the difference between the drive frequency and the LC frequency. Thus, the phase noise of the drive signal appearing at the LC frequency, which was considerable in the previous work, was reduced by up to 13.4 dB at the NMR frequency.

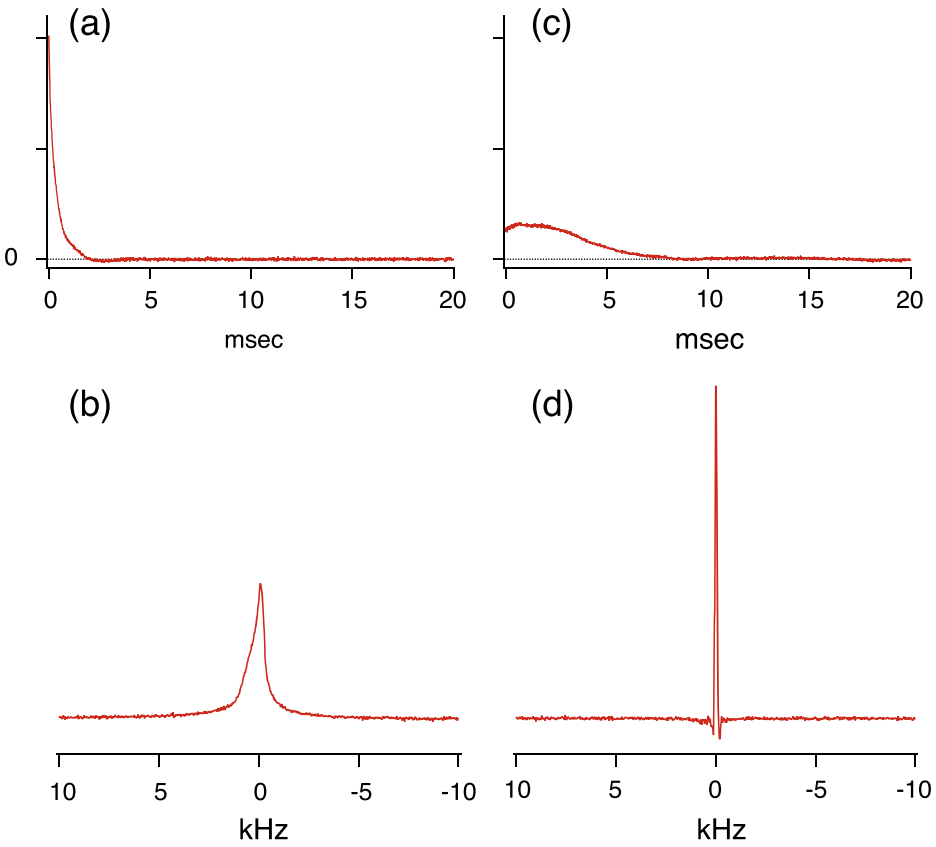

Fig. 9. (a) and (b) Single-pulse ^{1}H NMR signal and spectrum in 0.1 M aqueous solution of $CuSO_4$ acquired with the conventional electrical NMR detection scheme. (c) and (d) ^{1}H EMO NMR signal and spectrum obtained with the same sample. For both cases, signals were accumulated over 1000 times.

This led to significant enhancement of the signal-to-noise ratio of EMO NMR. The improvement reported here allowed us to explore the physics behind the process of signal transduction, including the study of the coherent nature of the nuclear induction signal affecting the mechanical perturbation on the membrane, and the transient response of the high-Q membrane oscillator.

The EMO NMR approach will find interest in field-sweep NMR experiments. In addition, the EMO approach would be a promising sensitive signal detection method in magnetic resonance imaging (MRI) performed by phase encoding. In phase encoded MRI, after application of rf and field-gradient pulses, measurements of the nuclear induction signal from the body under investigation are performed in highly homogeneous field where the resonance line is narrow enough for the EMO approach to be compatible with. Our future researches include development such a compact membrane-capacitor module that it can be installed inside superconducting magnets used for conventional NMR experiments.

Importantly, there still remains much room for improving the design of the membrane capacitor in terms of, e.g., the geometry of the electrodes and the gap length. In this work, the membrane-capacitor/mirror module was embedded in the $200 \times 200 \times 200$ mm vacuum chamber, and the compact 1 T permanent magnet was put aside the chamber to keep the capacitor module as close to the receiving coil as possible. Towards applications of EMO NMR to the conventional NMR system equipped with a high-field superconducting magnet, it will be necessary to design and fabricate a compact chamber such that it can be put inside the bore of the magnet. In addition, the gap d between the electrodes of the membrane capacitor may be aggressively reduced, because the electro-mechanical coupling strength increases as the inverse square of the gap, and thereby the electro-mechanical cooperativity, which measures the efficiency of signal communication between the hybrid systems against dissipation to environment, increases as d^{-4}; enhancement by an order of magnitude requires reduction in the capacitor gap by a factor of only $10^{-1/4} \sim 1.78$ [1]. Shorter capacitor gap is also advantageous in terms of the gain of the EMO transducer, which is given approximately by the electro-mechanical cooperativity times the opto-mechanical cooperativity [1]. The risk of high-voltage breakdown due to the excitation pulses could be diminished by improving the isolation between the excitation/detection coils. Such optimization would further increase the detection sensitivity of the EMO NMR approach. Moreover, since the width of the membrane spectrum increases with the electro-mechanical coupling, the spectral bandwidth that can be covered by the EMO NMR approach can also be enhanced without sacrificing the efficiency of rf-to-light signal upconversion.

The noise figure of our best preamplifier used in this work for room-temperature operation was 1.1 (noise temperature: 84 K). Conversely, in room-temperature EMO NMR demonstrated in this work, the noise figure of the membrane transducer can be made as low as 0.089 dB (noise temperature: 6 K) with realistic optimization [1]. If the entire detection system, including the coil and the membrane, is physically cooled down to cryogenic temperature, the present approach potentially offers superior noise performance compared to that of the state-of-art cryogenic NMR probes.

Since the higher membrane frequency is desirable, membranes with higher intrinsic frequency of mechanical oscillation or use of a higher order mode can be options. Potential problems include the smaller physical size of the membrane leading to the reduced capacitance, and the complexity of the pattern of the electrode.

It is also worth pointing out that the narrow-band nature of the EMO NMR approach is compatible with magnetometry in low fields.

Acknowledgment

We are grateful to Atsushi Noguchi, Rekishu Yamazaki, Eiji Iwase, Jacob M. Taylor, Yasunobu Nakamura, Kazuhiko Yamada, Masato Takahashi, Atushi Saito, and Kiyonori Takegoshi for fruitful discussions. This work has been supported by the SENTAN program (Grant No. 14537844) of Japan Science and Technology Agency and MEXT KAKENHI (Grant No. 18055012).

References

[1] K. Takeda, K. Nagasaka, A. Noguchi, R. Yamazaki, Y. Nakamura, E. Iwase, J.M. Taylor, K. Usami, Electro-mechano-optical detection of nuclear magnetic resonance, Optica 5 (2018) 152–158, https://doi.org/10.1364/OPTICA.5.000152.

[2] T. Bagci, A. Simonsen, S. Schmid, L.G. Villanueva, E. Zeuthen, J. Appel, J.M. Taylor, A. Sørensen, K. Usami, A. Schliesser, E.S. Polzik, Optical detection of radio waves through a nanomechanical transducer, Nature 507 (2014) 81–85, https://doi.org/10.1038/nature13029.

[3] K. Takeda, A highly integrated FPGA-based nuclear magnetic resonance spectrometer, Rev. Sci. Instrum. 78 (2007) 033103, https://doi.org/10.1063/1.2712940.

[4] K. Takeda, OPENCORE NMR: open-source core modules for implementing an integrated FPGA-based NMR spectrometer, J. Magnet. Reson. 192 (2008) 218–229, https://doi.org/10.1016/j.jmr.2008.02.019.

[5] K. Takeda, Highly customized NMR systems using an open-resource, home-built spectrometer, Ann. Rep. NMR Spectrosc. 74 (2011) 355–393, https://doi.org/10.1016/B978-0-08-097072-1.00007-8.

[6] F. Martin Ciurana, G. Colangelo, R.J. Sewell, M.W. Mitchell, Real-time shot-noise-limited differential photodetection for atomic quantum control, Opt. Lett. 41 (2016) 2946–2949, https://doi.org/10.1364/OL.41.002946, Available from: arXiv: 1605.03489.

[7] D. Wilson, C. Regal, S. Papp, H. Kimble, Cavity optomechanics with stoichiometric SiN films, Phys. Rev. Lett. 103 (2009) 207204, https://doi.org/10.1103/PhysRevLett.103.207204.

[8] D.M. Pozer, Microwave Engineering, fourth ed., John Wiley & Sons, 2011.

[9] D.B. Leeson, A simple model of feedback oscillator noise spectrum, Proc. IEEE 54 (1966) 329–330, https://doi.org/10.1109/9780470544952.ch6.

[10] M. Aspelmeyer, T.J. Kippenberg, F. Marquardt, Cavity optomechanics, Rev. Modern Phys. 86 (2014) 1391–1452, https://doi.org/10.1103/RevModPhys.86.1391.

[11] K. Takeda, N. Ichijo, Y. Noda, K. Takegoshi, Elemental analysis by NMR, J. Magnet. Reson. 224 (2012) 48–52, https://doi.org/10.1016/j.jmr.2012.09.004.

[12] K. Yamada, K. Kitagawa, M. Takahashi, Field-swept ^{33}S NMR study of elemental sulfur, Chem. Phys. Lett. 618 (2015) 20–23, https://doi.org/10.1016/j.cplett.2014.10.061.